Strong enhancement of the ferromagnetic phase and local order in Ru substituted manganites studied by EXAFS and dc magnetization measurements

C. Castellano[a,*], G. Berti[b], M. Ferretti[c], A. Martinelli[d], M.R. Cimberle[e]

[a]*Dipartimento di Chimica, Università degli Studi di Milano, via Golgi 19, 20133 Milano, Italy*
[b]*Dipartimento di Fisica, Politecnico di Milano, piazza Leonardo da Vinci 32, 20133 Milano, Italy*
[c]*Dip. Chimica e Chimica Industriale, Università di Genova, Via Dodecaneso 31, I-16146 Genova, Italy*
[d]*CNR-SPIN, C.so Perrone 24, 16152 Genova, Italy*
[e]*CNR-IMEM c/o Dipartimento di Fisica, Via Dodecaneso 33, I-16146 Genova, Italy*

*Corresponding author. Tel.: +39-0250314449; fax: +39-0250314454

E-mail address: carlo.castellano@unimi.it

Abstract

We report extended X-ray absorption fine structure (EXAFS) and dc magnetization measurements performed on $(La_{1-x}Ca_x)(Mn_{1-y}Ru_y)O_3$ samples (x = 0.37 and 0.75 and y = 0.03 or 0.08).

In the nanoscale phase inhomogeneity scenario characteristic of these complex oxides, we compare the effects induced by the partial substitution of Mn with mixed valence non-Jahn-Teller Ru^{5+} and at most very weak Jahn-Teller Ru^{4+} ions with those induced by the already studied analogous substitutions of Mn with non-Jahn-Teller Cr^{3+} or Ni^{2+} or Jahn-Teller Cu^{2+}.

We find evidence both from dc magnetization and EXAFS that the ruthenium doping induces a huge effect, clearly enhancing (more efficiently than is the case for the other dopants) the double exchange effect and consequently the metallic/ferromagnetic phase and the local structural order at the expenses of the charge-ordered phase component. In the x = 0.75 long-range charge-ordered system these effects are much more evident, as expected, while for x = 0.37 the magnetic ion partial substitution does not significantly modify the metal-insulator and ferromagnetic transitions, already present in the parent compound.

Keywords: A. Complex oxides; C. Inhomogeneous phase; D. magnetic measurements; D. EXAFS

1. Introduction

Perovskite manganites such as the solid solution $(La_{1-x}Ca_x)MnO_3$ present a complex phase diagram characterized, in the doping range $0.20 < x < 0.50$, by a transition from a high temperature paramagnetic insulating phase to a ferromagnetic (FM) metallic one, coupled with the so-called negative colossal magnetoresistance (CMR) effect [1,2]. On the other hand, for Ca dopings greater than 50 % the presence of charge ordering (CO) of Mn^{3+} and Mn^{4+} ions in different sublattices is observed ($T_{CO} < 260$ K, as a function of doping). Many theoretical models like the classical double exchange mechanism and a strong Jahn-Teller (J-T) charge-phonon polaronic coupling [3] have been proposed to explain the mechanism determining the CMR effect. Moreover, it was found experimental evidence of the presence of spin or magnetic polarons observing the formation in the paramagnetic matrix of local magnetically ordered regions of 12 Å starting from about 30 K below the Curie temperature T_C, where the charge carrier remains trapped as in a polaronic state [4]. In this framework, experimental evidences of an inhomogeneous phase, where metallic/ferromagnetic and insulating domains of nanometer dimensions coexist and percolate at low T, are reported in the literature for the hole-doped region of the $(La_{1-x}Ca_x)MnO_3$ phase diagram [5-8].

In the last years, beside the more and more diffused applicative and spintronic studies [9], the main research topic has been the identification of the nature of the insulating component in the inhomogeneous phase at low T for $0.20 < x < 0.50$; it could be a CO phase with a very low coherence length as such not detectable by many techniques, becoming more extended at Ca dopings greater than 50 %. In the same way it can be argued that at these high doping regimes ($x > 0.50$) a long-range CO phase, present in the phase diagram, and a fluctuating FM phase can always coexist at low T. Diffraction or other techniques sensitive only to long-range ordered structures do not evidence in each case the presence of the minority phase component whereas probably the comprehension and the control of this phase separation is at the bases of CMR.

In this general scenario, the partial substitution of the Mn magnetic ion amplifies one phase component with respect to the other, as shown in Refs. 10-16. This result is obtained due to the strong coupling between CO and J-T lattice distortion (induced by the presence of the Mn^{3+} ion or of its substitutes), as already evidenced by our EXAFS measurements performed on $(La_{0.25}Ca_{0.75})MnO_3$ [17]. Other interesting effects arise from the structural disorder induced by the different ionic radii of the cationic species located at the B site of the ABO_3 perovskite-type structure, and by the magnetic interaction between Mn and its dopants,

acting on the conduction bandwidth along the *B*-O-*B* bond paths. In addition, the dopant cationic species induce a re-equilibration of the $[Mn^{3+}]/[Mn^{4+}]$ ratio in order to maintain the electroneutrality.

In our previous papers [16-19] we studied samples of the family $(La_{1-x}Ca_x)(Mn_{1-y}M_y)O_3$ (with *M* = Ni, Cr, Cu, x = 0.37, 0.75 and y = 0.03 or 0.08) and the corresponding $(La_{1-x}Ca_x)MnO_3$ un-substituted compounds [17]. When substituting Mn with some percent of Cr^{3+} or Ni^{2+} we favoured the FM phase component at the expense of the CO one since both the substituting ions are not associated with a lattice J-T distortion thus resulting in an effective or site-random magnetic field [9,10]. As we foresaw, nickel and chromium, acting as random impurities, removed the CO features as observed both in magnetization, EXAFS and neutron diffraction measurements [14-18]. Moreover, for x < 0.50 the behaviour of the EXAFS parameters like the local order or Debye-Waller factor was strictly correlated to that of susceptibility and magnetization both in the ferromagnetic-paramagnetic transition temperature and in the width of the transition itself. This correlation confirmed the strong magnetoelastic coupling present in these materials between structural-polaronic and magnetic degrees of freedom. Anyway, our EXAFS results on the charge-ordered sample $(La_{0.25}Ca_{0.75})MnO_3$ before and after Mn substitution with Cr revealed how an enhanced local disorder still persists in $(La_{0.25}Ca_{0.75})(Mn_{0.92}Cr_{0.08})O_3$ probably strictly connected to a residual short-range CO phase, although reduced after Cr doping [18]. This residual effect was not observed on a macroscopic scale in the magnetization measurements performed on the same samples where the CO phase resulted to be completely removed. Therefore, only on a local scale, the effect of Cr was still not sufficient to strongly reduce the local disorder [18].

In successive papers [16,19], however, we evidenced the ability of the Jahn-Teller Cu^{2+} species to favour antiferromagnetism (AFM), CO and hence the super-exchange interactions, suppressing FM and enhancing the correlated local disorder. We found also that Mn substitution influences not only the CO phase but also the paramagnetic-ferromagnetic transition, which changes shape and temperature due to the changes in the balance between double exchange and superexchange interactions along the *B*-O-*B* conduction paths [18].

In this context, it is known that ruthenium is much more efficient than chromium in weakening CO since it induces higher T_C values and much broader metallic regions, as evidenced in Ref. 20 only by magnetization measurements. This high Ru efficiency for inducing ferromagnetism and metallicity has been explained in terms of the presence of two oxidation states Ru^{5+} and low spin Ru^{4+}, both exhibiting occupied t_{2g} and empty

e_g levels. The occurrence of this mixed Ru^{5+} - Ru^{4+} valence state in substituted manganites has been reported in several previous investigations [20-25]. More in general, in perovskites prepared in air or under oxygen, Ru^{5+} results to be very stable and some systems were shown to contain only this last species [26,27] or at most a valence fluctuation according to the equilibrium $Mn^{3+} + Ru^{5+} \leftrightarrow Mn^{4+} + Ru^{4+}$, thus increasing the Mn^{3+} content [20,28].

Moreover, the debate about the non-Jahn-Teller or rather very weak Jahn-Teller nature of the low spin Ru^{4+} ions is still open [29] but what is essential in our case is that the structural distortion is at most much smaller than in other doping cases. The electronic configuration and an orbital reorientation in the antiferromagnetic structures resulting from a ferromagnetic coupling between Ru^{5+}, Ru^{4+} and Mn^{3+} induce the double exchange more efficiently than Cr^{3+} (as evidenced by neutron diffraction on the electron doped side of a $(Sm_{0.2}Ca_{0.8})(Mn_{0.9}Ru_{0.1})O_3$ sample [28]). Moreover, Mn^{3+}/Mn^{4+} electronic fluctuations around mixed valence Ru, strongly enhance the formation of percolating metallic clusters explaining the appearance of metallicity and FM in the phase separation framework. As a result, in addition to the hindering of CO and the induction of FM, an insulator to metal transition is obtained as the ruthenium content increases reaching the percolation threshold with the decrease of the insulating AFM component [20,28].

Therefore, following the guideline of our extended X-ray absorption fine structure (EXAFS) study on the series of Mn substituted samples, we are interested in presenting and comparing the effects induced on the magnetic phase, local order and structure by the Mn/Ru substitution, as a function of temperature, in $(La_{0.25}Ca_{0.75})(Mn_{0.92}Ru_{0.08})O_3$, $(La_{0.25}Ca_{0.75})(Mn_{0.97}Ru_{0.03})O_3$, $(La_{0.63}Ca_{0.37})(Mn_{0.92}Ru_{0.08})O_3$ and $(La_{0.63}Ca_{0.37})(Mn_{0.97}Ru_{0.03})O_3$, with those obtained in the previously studied Cr, Ni, Cu substituted samples [18,19]. The pristine compound $(La_{0.63}Ca_{0.37})MnO_3$ is metallic and ferromagnetic below T_C = 270 K, while on the other side of the phase diagram $(La_{0.25}Ca_{0.75})MnO_3$ exhibits CO below T_{CO} = 225 K.

All the samples were also characterized by dc magnetization measurements.

2. Experimental methods and data analysis

Polycrystalline $(La_{1-x}Ca_x)(Mn_{1-y}Ru_y)O_3$ samples were prepared by means of a solid state reaction: binary oxides (CaO 99.95% ALDRICH; La_2O_3 99.99% ALFA AESAR; MnO_2 99.999% ALFA AESAR, RuO_2 99.998%

ALFA AESAR) were firstly sieved (80 mesh), then mixed in stoichiometric amounts and finally reacted at high temperature in air. Four thermal treatments with intermediate grinding were carried out, the first at 1523 K for 15 h and the remaining ones at 1603 K for 18 h. X-ray powder diffraction data (XRPD; PHILIPS PW1830; Bragg-Brentano geometry; CuK_α; secondary monochromator; 2θ range: 13 - 80°; step: 0.020° 2θ; sampling time: 15 sec) were acquired.

The EXAFS studied samples were pellets of polycrystalline powders dispersed in a cellulose matrix optimising the jump at the absorption edge. The Mn K-edge (6539 eV) EXAFS data were recorded in transmission geometry on beamline E4 at the HASYLAB synchrotron radiation source (Hamburg) using a double-crystal Si(111) monochromator and a helium flux cryostat. In order to accurately follow the behavior of the local order and structure parameters as a function of temperature, we measured accurate spectra at different temperatures between 10 and 295 K (Fig. 1). The EXAFS data were reduced using the Demeter package standard procedures [30]; fits of the k^3 weighted EXAFS data were carried out in r space using theoretical functions from the FEFF9 code [31]. Examples of the resulting high-quality k-space data at several temperatures and up to 16 $Å^{-1}$ are shown in Fig. 1. Starting from the orthorhombic unit cell model typical of Jahn-Teller distorted manganites, the FEFF code computes overlapping muffin tin spherically symmetric potentials and their corresponding phase-shifts thus generating the different path contributions in order to fit the data.

The starting models are the same already reported in previous papers for the corresponding un-substituted compounds [17,18].

To include the first and further neighbours in the data (full fit range: 1.05–3.65 Å), we used the first shell Mn-O peak with bond length R = 1.95 Å and coordination number N = 6, at 298 K, the longer peaks: Mn-La (N = 2 and R = 3.25 Å), Mn-La (N = 6 and R = 3.36 Å) and Mn-Mn (N = 6, R = 3.85 Å), the double scattering Mn-O-Mn (N = 12), the triple forward scattering through the absorber $Mn\text{-}O_{(1)}\text{-}Mn\text{-}O_{(1)}$ (N = 6) and the triple forward triangle $Mn\text{-}O_{(2)}\text{-}Mn\text{-}O_{(2)}$ (N = 6).

The initial fitting parameters were the Debye-Waller factors σ^2, the interatomic bond lengths R, the E_0 shift in the edge energy with respect to the theoretical value, and the amplitude reduction factor S_0^2 from multielectron effects. This last factor is generally between 0.8 and 1.0. At low temperature, the lattice is well ordered, and S_0^2 was determined from the average of several fits to scans at 50 K and fixed at 0.91. The E_0

shift was also constrained to a single value for all the paths. The coordination numbers were fixed as described above. In this way, the uncertainty on the Debye-Waller factors σ^2 was reduced [19].

The dc magnetic measurements were performed by using a commercial magnetometer (MPMS by Quantum Design) on the same powder samples.

3. Results and discussion

The structural refinements carried out using the XRPD data evidence that all the samples crystallize in the orthorhombic *Pnma* structure characterizing the pure (La,Ca)MnO_3 parent compound; remarkably, no evidence for secondary phases is detected. Figure 2 shows the Rietveld refinement plot obtained for the sample $(La_{0.25}Ca_{0.75})(Mn_{0.92}Ru_{0.08})O_3$ at 300 K, selected as representative (R_{Bragg}: 3.54%). Moreover, structural refinement confirms that Ru actually substitutes Mn.

We present here the EXAFS local structure parameters as retrieved from the analysis described in the previous section and the dc magnetization behaviour of the four cited Ru-substituted and pristine compounds in order to point out and verify the huge role of this magnetic ion substitution. Zero field cooled (ZFC) and FC susceptibility measurements performed on the substituted samples, with $x = 0.75$, $x = 0.37$ are shown in Fig. 3 and Fig. 4, respectively.

In the $(La_{0.25}Ca_{0.75})(Mn_{0.92}Ru_{0.08})O_3$ sample, the increasing of the ferromagnetic phase results to be very marked with respect to the $(La_{0.25}Ca_{0.75})(Mn_{0.92}Ru_{0.03})O_3$ composition (see Fig. 2) and also compared to the parent $(La_{0.25}Ca_{0.75})MnO_3$ CO sample for which we reported in Refs. 18 and 19 the characteristic CO susceptibility drop determined by the appearance of antiferromagnetic superexchange interactions correlated with the localization of charge carriers. The non-J-T Ru^{5+} and very weak J-T Ru^{4+} substituting ions act as random impurities determining an effective or site-random magnetic field and favouring the formation of an important ferromagnetic – metallic component over the CO one.

Regarding the $(La_{0.63}Ca_{0.37})(Mn_{0.92}Ru_{0.08})O_3$ and $(La_{0.63}Ca_{0.37})(Mn_{0.92}Ru_{0.03})O_3$ samples we show in Fig. 3 that after the substitution of Mn with Ru a main ferromagnetic phase remains, though the magnetic transition is

slightly shifted to lower temperatures and above all broadened. The unsubstituted sample presents a ferromagnetic–metallic phase below T_C = 270 K probably coexisting with a weaker insulating and CO component [19]. The phase transition results to be steeper in the $(La_{0.63}Ca_{0.37})(Mn_{0.92}Ru_{0.08})O_3$ case due to the higher ruthenium content (Fig. 4).

Therefore from a macroscopic point of view our starting hypotheses are verified: the ferromagnetic state is favoured in presence of non-Jahn-Teller or very weak Jahn-Teller substituting ions and ruthenium is very efficient for this purpose.

We describe now the behaviour of the structural EXAFS parameters, focusing our attention on the Mn-O first shell.

In Fig. 5 the local order or Debye-Waller parameter σ^2 of the MnO_6 first coordination shell is reported as a function of temperature for the Mn-substituted samples $(La_{0.25}Ca_{0.75})(Mn_{0.92}Ru_{0.08})O_3$, $(La_{0.25}Ca_{0.75})(Mn_{0.97}Ru_{0.03})O_3$, and for the pristine $(La_{0.25}Ca_{0.75})MnO_3$ compound.

We show that the Mn/Ru substitution determines a slight decrease in the local disorder with respect to the undoped sample for y = 0.03 whereas the effect is much more evident when the ruthenium content increases to y = 0.08. This last doping effect is so marked that the σ^2 trend for y = 0.08 perfectly superimposes the fit (Fig. 5, continuous line) performed at high temperatures (above T_{CO}) to a temperature dependent correlated Debye-like behavior σ_D^2, with a correlated Debye temperature θ_D of about 510 K, plus a temperature independent static contribution σ^2_S = 0.00854 Å^2 due to the presence of the Jahn-Teller Mn^{3+} distorted environment. The high temperature fitted Debye-Waller factor $\sigma^2(T) = \sigma^2_D + \sigma^2_S$, as already explained in previous papers [17-19], is usually a good approximation for all the phonon modes [32,33]. Therefore, the ruthenium doping tends to cancel almost completely the additional local disorder due to charge ordering [17]. Differently, in our previous paper (Ref. 18), we showed how the Mn/Cr substitution only slightly reduces the higher local disorder related to the charge-ordered phase. Therefore, the Mn/Ru substitution results to be much more efficient also from the study of the local structure parameters.

For what concerns the $(La_{0.63}Ca_{0.37})(Mn_{0.92}Ru_{0.08})O_3$ and $(La_{0.63}Ca_{0.37})(Mn_{0.97}Ru_{0.03})O_3$ samples we evidence in Fig. 6, after comparison with $(La_{0.63}Ca_{0.37})MnO_3$, that the local order parameter σ^2 suddenly decreases and substantially remains similar to that of a metallic/ferromagnetic system [34], in agreement with the magnetization results. The magnetic substitution with ruthenium ions does not influence the already

predominant ferromagnetic/metallic and less disordered phase present at these doping levels, since it goes in the same phase diagram direction.

Moreover, for all the samples we have obtained six identical Mn-O interatomic distances (Fig. 6) also due to the EXAFS resolving power between two scattering shells involving the same chemical species at different distances. Since the maximum k vector for our data is k_{max} = 16 Å^{-1}, we can accurately resolve splittings of

$\Delta R > \pi/2k_{max} \sim 0.098$ Å [35,36] and our case is well beyond this EXAFS ability to resolve splitted peaks. Therefore, even if a ΔR below 0.098 Å was present, we would not be able to rigorously point it out. The resulting bond lengths are also almost independent of temperature and quite coinciding with each other within the statistical error, at a fixed Ca content (Fig. 7). The Mn-O bond lengths for x = 0.75 are slightly shorter than for x = 0.37, in accordance with the available crystallographic data files.

The ruthenium substitution effect is evident also in these bond lengths results since in the undoped compounds we always revealed a bimodal distribution of the six Mn-O distances of the MnO_6 octahedra indicating a clear distortion [17,37] that results to be mostly removed after this partial substitution.

It is worth noting that the Mn site partial substitution with non-Jahn-Teller ions like Cr^{3+} and Ni^{2+} was not able to completely remove this octahedron distortion, strictly related to charge ordering and localization [18]. Therefore the particular aptitude of Ru of promoting a FM metallic and more ordered state is confirmed also by these results on the interatomic distances.

4. Conclusions

We found the evidence of a strong enhancement of the FM long-range phase component and consequent local disorder decrease after the Mn/Ru partial substitution, above all in the $(La_{0.25}Ca_{0.75})(Mn_{0.92}Ru_{0.08})O_3$ sample. Moreover, the same FM phase is only slightly influenced in the already ferromagnetic x = 0.37 systems.

Accordingly, the local structure parameters obtained from EXAFS still confirm, in the former compound, the almost complete disappearance of the additional local disorder related to the pristine charge-order phase

component, and ruthenium results to be, due to its electronic and spin configuration, the most effective dopant on the manganese magnetic site in a nanometric phase separation context [38].

Acknowledgments

The authors thank E. Welter for technical support at HASYLAB. This work was supported by the European Community – Research Infrastructure Action under the FP6 "Structuring the European Research Area" Programme (through the Integrated Infrastructure Initiative "Integrating Activity on Synchrotron and Free Electron Laser Science").

References

[1] P. Schiffer, P.A. Ramirez, W. Bao, S.-W. Cheong, Phys. Rev. Lett. 75 (1995) 3336.

[2] C. Zener, Phys. Rev. 82 (1951) 403.

[3] A. J. Millis, P.B. Littlewood, B.I. Shraiman, Phys. Rev. Lett. 74 (1995) 5144.

[4] J. M. De Teresa, M.R. Ibarra, P.A. Algarabel, C. Ritter, C. Marquina, J. Blasco, J. Garcia, A. del Moral, Z. Arnold, Nature 386 (1997) 256.

[5] A. Moreo, S. Yunoki, and E. Dagotto, Science 283 (1999) 2034.

[6] M. Fäth, S. Freisem, A.A. Menovsky, Y. Tomioka, J. Aarts, J.A. Mydosh, Science 285 (1999) 1540.

[7] F. Cordero, C. Castellano, R. Cantelli, M. Ferretti, Phys. Rev. B 65 (2002) 124031.

[8] P. Levy, F. Parisi, M. Quintero, L. Granja, J. Curiale, J. Sacanell, G. Leyva, G. Polla, R.S. Freitas and L. Ghivelder, Phys. Rev. B 65 (2002) 140401.

[9] B. B. Chen, P. F. Chen, H. R. Xu, X. L. Tan, F. Jin, Z. Guo, B. W. Zhi, and W. B. Wu, Appl. Phys. Lett. 104 (2014) 242416.

[10] T. Katsufuji, S.-W. Cheong, S. Mori and C.H. Chen, J. Phys. Soc. Jap. 68 (1999) 1090.

[11] H. Oshima, Y. Ishihara, M. Nakamura, K. Miyano, Phys. Rev. B 63 (2001) 094420, and references therein.

[12] T. S. Zhao, W.X. Xianyu, B.H. Li, Z.N. Qian, J. Alloys Compd. 459 (2008) 29.

[13] Xingmei Shen, Guoyue Xu, Chunming Shao, J. Alloys Compd. 499 (2010) 212.

[14] A. Martinelli, M. Ferretti, C. Castellano, M.R. Cimberle, M. Tropeano, C. Mondelli, C. Ritter, Phys. Rev. B 73 (2006) 064423.

[15] A. Martinelli, M. Ferretti, C. Castellano, M.R. Cimberle, C. Ritter, J. Phys.: Condens. Matter 20 (2008) 145210.

[16] A.Martinelli, M. Ferretti, C. Castellano, M. R. Cimberle, C. Ritter, Journal of Solid State Chemistry 200 (2013) 128.

[17] C. Castellano, A. Paolone, F. Cordero, R. Cantelli, M. Ferretti, Solid State Commun. 129 (2004) 143.

[18] C. Castellano, F. Cordero, O. Palumbo, R. Cantelli, R. Cimberle, M. Tropeano, A. Martinelli, M. Ferretti, Solid State Commun. 136 (2005) 244.

[19] C. Castellano, M. Ferretti, A. Martinelli, M.R. Cimberle, J. Alloys Compd. 478 (2009) 479.

[20] B. Raveau, A. Maignan, C. Martin, R. Mahendiran, and M. Hervieu, J. Solid State Chem. 151 (2000) 330.

[21] S. S. Manoharan, H. L. Ju, K. M. Krishnan, J. Appl. Phys. 83 (1998) 7183.

[22] B. Raveau, A. Maignan, R. Mahendiran, D. Khomskii, C. Martin, S. Hébert, M. Hervieu and R. Frésard, J. Phys. Chem. Solids 63 (2002) 901.

[23] Brajendra Singh , Ranjan K. Sahu , S. Sundar Manoharan , K. Dörr and K. -H. Müller, J. Magn. Magn. Mater. 270 (2004) 358.

[24] A. I. Shames, E. Rozenberg, C. Martin, A. Maignan, B. Raveau, G. André, and G. Gorodetsky, Phys. Rev. B 70 (2004) 134433.

[25] V. P. S. Awana, S. Ichihara, J. Nakamura, M. Karppinen, H. Yamauchi, Jinbo Yang, W. B. Yelon, W. J. James, S. K. Malik, J. Appl. Phys. 91 (2002) 8501.

[26] P. D. Battle and C. W. Jones, J. Solid State Chem. 78 (1989) 108.

[27] P. D. Battle, J. C. Gibb, C. W. Jones, and F. Studer, J. Solid State Chem. 78 (1989) 281.

[28] C. Martin, A. Maignan, M. Hervieu, C. Autret, B. Reveau, D.I. Khomskii, Phys. Rev. B 63 (2001) 174402.

[29] J. van Duijn, R. Ruiz-Bustos, A. Daoud-Aladine, Phys. Rev. B 86 (2012) 214111.

[30] B. Ravel and M. Newville, J. Synchrotron Radiat. 12 (2005) 537.

[31] A. L. Ankudinov, B. Ravel, J.J. Rehr, and S.D. Conradson, Phys. Rev. B 58 (1998) 7565.

[32] G. Beni and P. M. Platzmann, Phys. Rev. B 14 (1976) 1514.

[33] N. W. Ashcroft and N. D. Mermin, in *Solid State Physics* (Saunders College, Philadelphia, 1976).

[34] C.H. Booth, J. Bridges, G.H. Kwei, J.M. Lawrence, A.L. Cornelius and J.J. Neumeier, Phys. Rev. B 57 (1998) 10440.

[35] P. A. Lee, P. H. Citrin, P. Eisenberger, and B. M. Kincaid, Rev. Mod. Phys. 53 (1981) 769.

[36] T. Keiber, F. Bridges, and B. C. Sales, Phys. Rev. Lett. 111 (2013) 095504.

[37] A. Paolone, C. Castellano, R. Cantelli, G. Rousse, and C. Masquelier, Phys. Rev. B 68 (2003) 014108.

[38] A. Sendil Kumar, Ravinder Reddy K, Anil K. Bhatnagar, J. Alloys Compd. 639 (2015) 139.

Figure Captions

Fig. 1. EXAFS $k\chi(k)$ signal of $(La_{0.63}Ca_{0.37})(Mn_{0.92}Cu_{0.08})O_3$ as a function of temperature between 50 K (lower curve) and 295 K (upper curve).

Fig. 2. Rietveld refinement plot for $(La_{0.25}Ca_{0.75})(Mn_{0.92}Ru_{0.08})O_3$ (XRPD data at 300 K): the points in the upper field represent the observed intensity data, the calculated pattern is superposed and drawn as a solid line; the small vertical bars indicate the position of the allowed Bragg reflections; the difference between the observed and calculated patterns is plotted in the lower field.

Fig. 3. Temperature dependence of dc magnetization measured in ZFC and FC conditions with an external applied field $\mu_0 H = 0.05$ Tesla for $(La_{0.25}Ca_{0.75})(Mn_{0.97}Ru_{0.03})O_3$ (gray squares), $(La_{0.25}Ca_{0.75})(Mn_{0.92}Ru_{0.08})O_3$, (black squares) and $(La_{0.25}Ca_{0.75})MnO_3$ (rhombs).

Fig. 4. Temperature dependence of ZFC (full symbols) and FC (empty symbols) dc magnetization with an external applied field $\mu_0 H = 0.05$ Tesla for $(La_{0.63}Ca_{0.37})(Mn_{0.92}Ru_{0.03})O_3$ (gray squares), $(La_{0.63}Ca_{0.37})(Mn_{0.92}Ru_{0.08})O_3$ (black squares) and $(La_{0.63}Ca_{0.37})MnO_3$ (rhombs).

Fig. 5. Mn-O mean square relative displacement $\sigma^2(Å^2)$ of $(La_{0.25}Ca_{0.75})(Mn_{0.92}Ru_{0.08})O_3$ (full squares), $(La_{0.25}Ca_{0.75})(Mn_{0.97}Cu_{0.03})O_3$ (empty squares) and of the pristine $(La_{0.25}Ca_{0.75})MnO_3$ sample (full stars; adapted from Ref. 17), determined from the single shell analysis as a function of temperature (the continuous line represents the correlated Debye-like behaviour plus a static contribution to the total disorder factor).

Fig. 6. Mn-O mean square relative displacement $\sigma^2(Å^2)$ of $(La_{0.63}Ca_{0.37})(Mn_{0.92}Ru_{0.08})O_3$ (full squares), $(La_{0.63}Ca_{0.37})(Mn_{0.97}Ru_{0.03})O_3$ (empty squares) and of the pristine $(La_{0.63}Ca_{0.37})MnO_3$ sample (full stars; adapted from Ref. 18), determined from the single shell analysis as a function of temperature.

Fig. 7. Mn-O bond lengths ($N_{Mn\text{-}O} = 6$) of all the samples as a function of temperature.

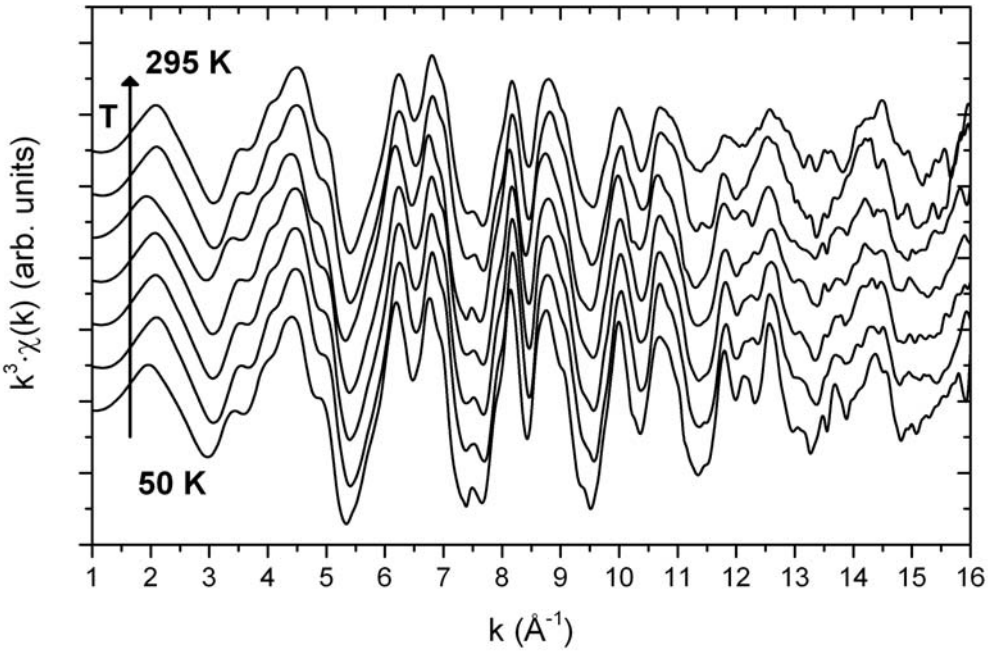
295 K
T
50 K
k³·χ(k) (arb. units)
k (Å⁻¹)

Fig. 1.

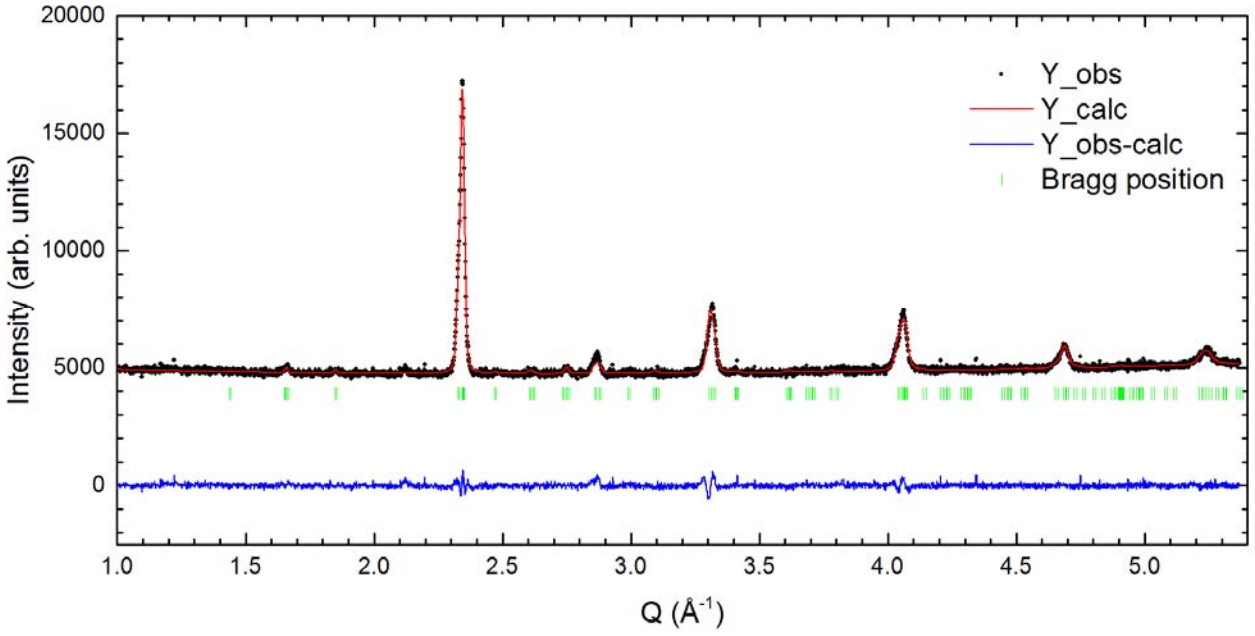
Y_obs
Y_calc
Y_obs-calc
Bragg position
Intensity (arb. units)
Q (Å⁻¹)

Fig. 2.

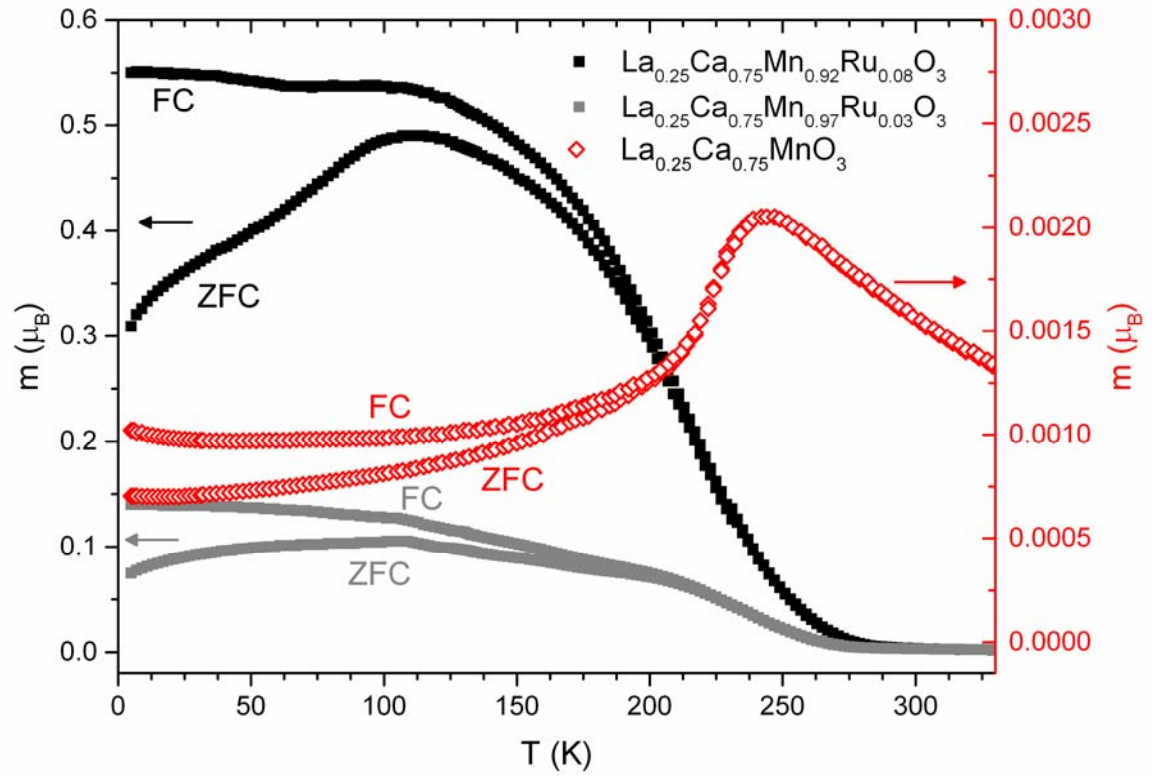
La0.25Ca0.75Mn0.92Ru0.08O3
La0.25Ca0.75Mn0.97Ru0.03O3
La0.25Ca0.75MnO3
FC
ZFC
FC
ZFC
FC
ZFC
m (μB)
m (μB)
T (K)
0.6
0.5
0.4
0.3
0.2
0.1
0.0
0.0030
0.0025
0.0020
0.0015
0.0010
0.0005
0.0000
0
50
100
150
200
250
300

Fig. 3.

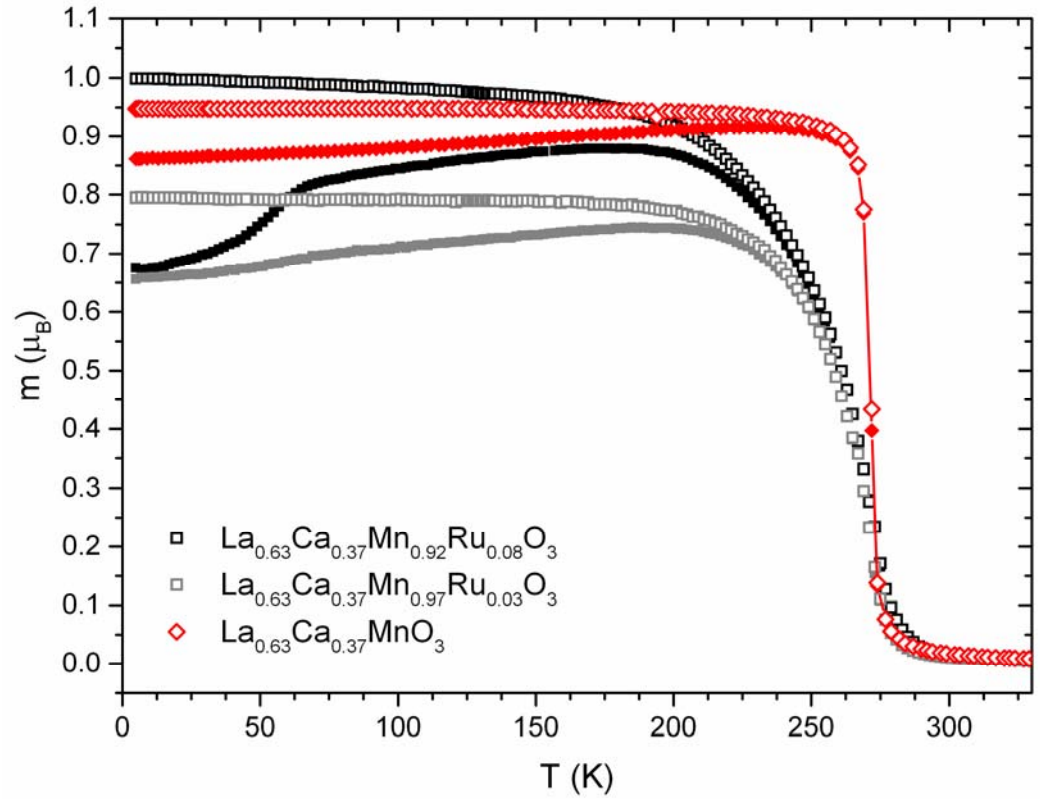
m (μ_B)
T (K)
$La_{0.63}Ca_{0.37}Mn_{0.92}Ru_{0.08}O_3$
$La_{0.63}Ca_{0.37}Mn_{0.97}Ru_{0.03}O_3$
$La_{0.63}Ca_{0.37}MnO_3$

Fig. 4.

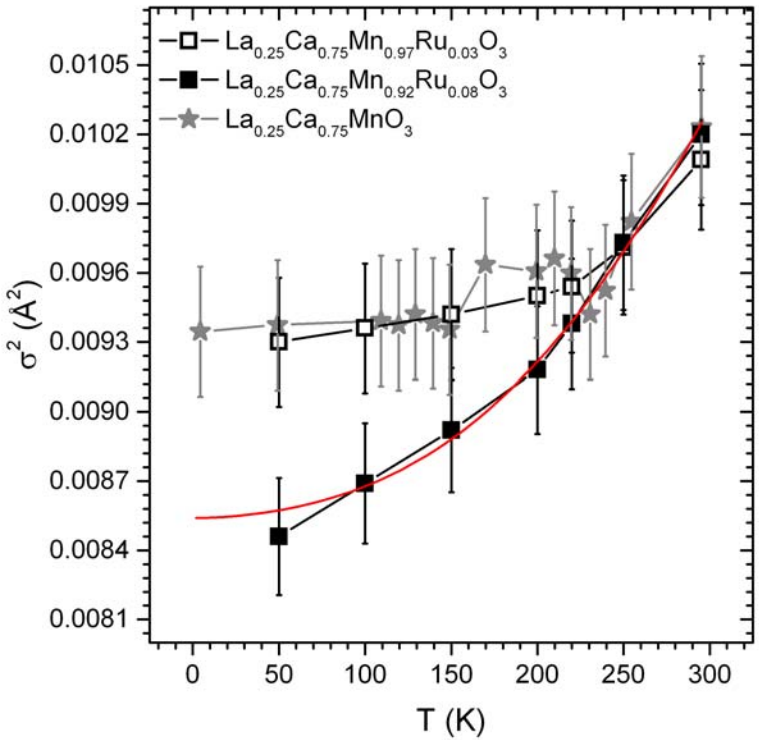
σ^2 (Å^2)
T (K)
$La_{0.25}Ca_{0.75}Mn_{0.97}Ru_{0.03}O_3$
$La_{0.25}Ca_{0.75}Mn_{0.92}Ru_{0.08}O_3$
$La_{0.25}Ca_{0.75}MnO_3$

Fig. 5.

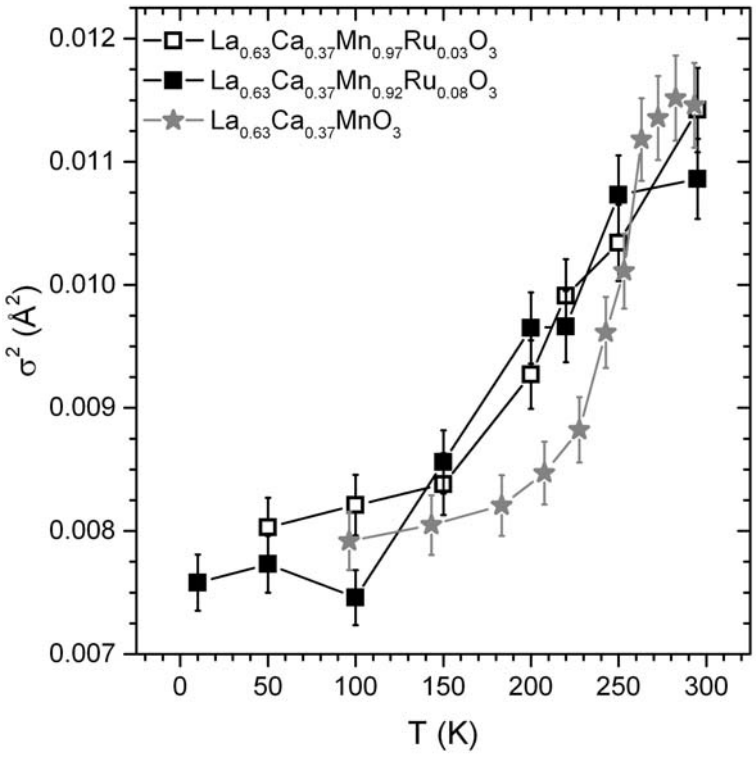
La0.63Ca0.37Mn0.97Ru0.03O3
La0.63Ca0.37Mn0.92Ru0.08O3
La0.63Ca0.37MnO3
σ2 (Å2)
T (K)

Fig. 6.

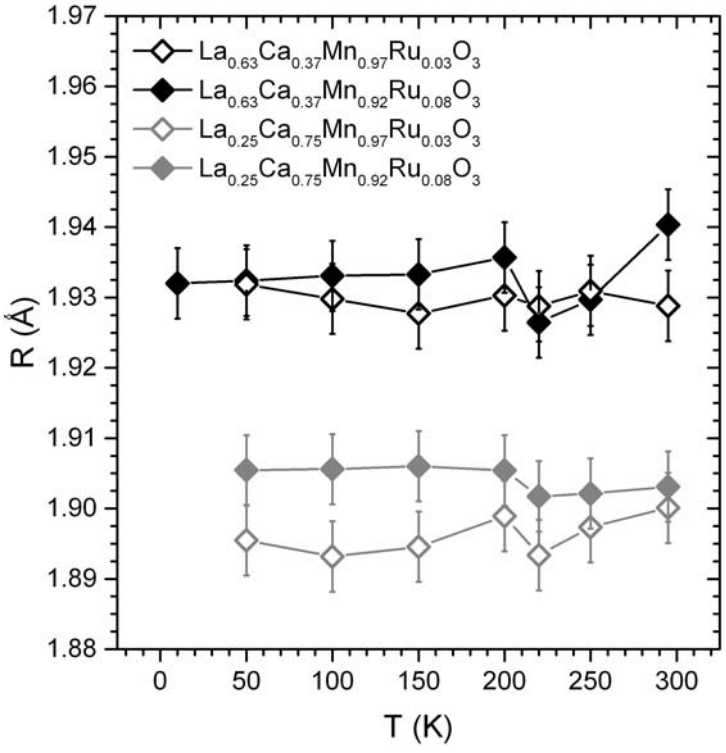
La0.63Ca0.37Mn0.97Ru0.03O3
La0.63Ca0.37Mn0.92Ru0.08O3
La0.25Ca0.75Mn0.97Ru0.03O3
La0.25Ca0.75Mn0.92Ru0.08O3
R (Å)
T (K)

Fig. 7.